Dimensionality reduction of non-buoyant microconfined high-pressure transcritical fluid turbulence

Lluís Jofre[a,*], Marc Bernades[a], Francesco Capuano[a]

[a]*Department of Fluid Mechanics, Universitat Politècnica de Catalunya · BarcelonaTech (UPC), Barcelona 08034, Spain*

Abstract

This work utilizes a novel data-driven methodology to reduce the dimensionality of non-buoyant microconfined high-pressure transcritical fluid turbulence. Classical dimensional analysis techniques are limited by the non-uniqueness of scale-free groups and the lack of a general strategy for quantifying their importance. Instead, the data-driven approach utilized is based on augmenting Buckingham's π theorem with ideas from active subspaces to overcome these limitations. Through this methodology, a principal dimensionless group has been identified that efficiently describes the behavior of the system in terms of normalized bulk turbulent kinetic energy. Additionally, a simplified version of the new dimensionless group is proposed, which presents the structure of a Reynolds number augmented with dynamic viscosity, thermal conductivity, or equivalently Prandtl number and isobaric heat capacity, and specific gas constant to account for thermophysical effects. Finally, the results obtained in this study, which is based on a realistic regime inspired by nitrogen at high-pressure microfluidic conditions, can be generalized to

---

*Corresponding Author
    Email address: `lluis.jofre@upc.edu` (Lluís Jofre)

other fluids using the principle of corresponding states.

Keywords: Dimensionality reduction, Microfluidics, Supercritical fluids, Turbulence

Nomenclature

Latin letters

a, b, c coefficients of the Peng-Robinson equation of state

c_P isobaric specific heat capacity

D_h hydraulic diameter

E total energy

Ec Eckert number

k turbulent kinetic energy

$\mathcal{M}$ dipole moment

Ma Mach number

P pressure

Pr Prandtl number

$\mathbf{q}$ heat flux vector

Q quantity of interest

Re Reynolds number

R_u universal gas constant

R' specific gas constant

sos   speed of sound

t time

T temperature

u streamwise velocity component

v wall-normal velocity component

$\bar{v}$ molar volume

2

v	velocity vector
w	spanwise velocity component
W	molecular weight
x	streamwise spatial coordinate
y	wall-normal spatial coordinate
z	spanwise spatial coordinate
Z	compressibility factor

Greek symbols

$\hat{\gamma}$	real-gas heat capacity ratio
δ	channel half-height
κ	thermal conductivity
κ_a	association factor
μ	dynamic viscosity
ν	kinematic viscosity
π	dimensionless group
ρ	density
$\boldsymbol{\tau}$	viscous stress tensor
ω	acentric factor

Main subscripts

b	bulk quantity
c	critical point
cw	cold wall
hw	hot wall
r	reduced quantity
w	wall

1. Introduction

High-pressure supercritical fluids are used in a wide range of engineering applications, like for example in gas turbines, supercritical water-cooled reactors and liquid rocket engines. They operate within high-pressure thermodynamic spaces in which intermolecular forces and finite packing volume effects become important. In this regard, it is important to distinguish between supercritical gas-like and liquid-like fluids separated by the pseudo-boiling line [1, 2]: (i) a supercritical liquid-like fluid is one whose density is large, and whose transport coefficients behave similar to a liquid; whereas (ii) the density of supercritical gas-like fluids is smaller, and their transport coefficients vary similar to gases. This set of thermophysical characteristics presents very interesting properties that can be leveraged to achieve turbulent flow regimes in microfluidic devices [3]. This is particularly important since, as in most macroscale energy applications related to power and heat transfer [4], turbulence is a key mechanism for achieving higher levels of performance and efficiency due to the notable increase in mixing and transfer rates it provides.

The novel approach mentioned above to achieve microconfined turbulence, which is considered also in this work, is based on operating under high-pressure transcritical conditions to leverage the hybrid thermophysical properties of supercritical fluids. In particular, the strategy proposed makes use of the rapid smooth transition of thermophysical properties across the pseudo-boiling line to tune supercritical fluids to present liquid-like densities [$\rho \sim 10^3$ kg/m^3] and gas-like viscosities [$\mu \sim 10^{-5}$ Pa·s], and therefore achieve $Re_b \sim 10^3 - 10^4$ for typical microfluidic velocities and channel sizes, and favoring, in this manner, inertial over viscous forces and resulting in turbulent flow. Focusing on the thermophysical properties of different supercritical fluids, this approach has been recently explored by Bernades et al. [5, 6]. The analyses presented in their work indicate that microconfined turbulent flow regimes can be potentially achieved by operating in the vicinity of the pseudo-boiling region for a wide range of popular working fluids, like for example carbon dioxide, methane, nitrogen, oxygen and water. In connection with this strategy, Zhang et al. [7] explored mixing intensification for antisolvent processes by operating at high pressures in free-shear coflow configurations at isothermal conditions. Nonetheless, the overall strategy is significantly different to the one studied in this work as: (i) jet flows

4

are inherently unstable, and consequently laminar-to-turbulent transition occurs in the range $Re_b \approx 30 - 2000$ [8]; (ii) coflows require complex microfluidic configurations; and (iii) isothermal conditions are not generally suitable for energy-related applications.

However, the analysis, design and optimization of microconfined high-pressure supercritical turbulent flow applications generally involves the understanding and characterization of a large variety of phenomena. In this regard, the challenge of operating with such complex systems is typically reduced by transforming the problem of interest into its dimensionless form. To this end, dimensional analysis provides a compelling framework to perform the operations required, as well as support for analyzing the resulting scale-free system. Its underlying principle is based on the notion of similarity, which postulates that relationships between physical quantities do not vary if the measurement units are changed. This central result implies that simpler small-scale experiments can be utilized to study larger-scale phenomena. In addition, one major advantage is that dimensional analysis typically yields a smaller number of independent variables than the original measured quantities. Hence, the dimensionality of the system is reduced, and as a result fewer (potentially expensive) experiments are needed to characterize its response, i.e., quantity of interest (QoI), to a set of inputs. For example, under particular conditions and simplifications, there is a direct relationship between the movement of large masses of air in the atmosphere and the motion of a fluid in a small-scale laboratory (or computational) model. The challenges are to find (i) those conditions and (ii) the transformation between them; in this case, the same ratio of inertial to viscous forces, i.e., Reynolds number. Dimensional analysis aims to help solve these two challenges in general problems by providing a set of mathematical techniques and methodologies.

The main utility of dimensional analysis results from its ability to contract the functional form of physical relationships. In problems for which a set of equations can be formulated to describe the physics, similarity can be inferred by normalizing all the equations in terms of quantities that characterize the problem, to subsequently identify the dimensionless groups that appear in the resulting dimensionless equations. This is an inspectional form of similarity analysis. This type of approach takes advantage of the complete mathematical description of the problem, typically revealing a higher degree of

similarity than a blind, less informed, dimensional analysis, and therefore provides more powerful insight. Dimensional analysis is, however, the only option in problems where the flow equations conditions are not fully available, and always useful because it is simple to apply and rapid in providing valuable insight.

The main result of dimensional analysis is the Buckingham's π theorem [9], which states that the form of any physics-based description of a system, e.g., conservation equations and experimental correlations, must be such that the relationship between the actual physical quantities remains valid independently of the magnitudes of the base units utilized. This feature provides a number of very useful outcomes in terms of (i) facilitating the inference of similarity laws, (ii) producing a basis for out-of-scale modeling, (iii) providing support for dimensionality reduction [10], and (iv) obtaining insight that is independent of the system of units utilized. However, as any other scientific approach, it presents some limitations. For example, (i) an incomplete, or unnecessary, set of independent variables may significantly complicate the analysis [11], (ii) the framework is not robust to external simplifying assumptions, (iii) the set of scale-free relations obtained is not unique, and (iv) there is no formal approach for quantifying the relative importance between dimensionless groups. In this regard, this work proposes to utilize a data-driven methodology inspired by the work of Constantine et al. [12] and adapted to multiphysics turbulent flows by Jofre et al. [13], which is aimed at addressing the last two shortfalls by means of augmenting Buckingham's π theorem with ideas developed in the field of active subspaces.

As previously introduced, the exploration and analysis of complex systems, specifically high-pressure supercritical turbulent flow problems, can be systematically approached by considering the important dimensionless groups characterizing the relations between the underlying physics phenomena. Extraction of the dimensionless parameters is also very useful for engineering practice as it allows one to identify important directions in the input space for the efficient design and optimization of systems. Therefore, the objective of this work is to utilize a novel semi-empirical methodology to effectively infer important dimensionless groups from data synthetically generated using direct numerical simulations of a channel flow problem to characterize important dimensionless groups in non-buoyant microconfined high-pressure supercritical fluid turbulence. The paper is organized as fol-

lows. In Section 2, the physics modeling and computational approach utilized to study supercritical fluids turbulence are described. A detailed presentation of the data-driven dimensional analysis methodology is given in Section 3. In Section 4, the configuration of the model problem is described in terms of physics, setup, and system parameters. Next, in Section 5, results and their analysis are discussed. Finally, the work is concluded and future directions are proposed in Section 6.

2. Flow physics and numerical modeling

The framework utilized for studying supercritical fluids turbulence in terms of (i) equations of fluid motion, (ii) real-gas thermodynamics, (iii) high-pressure transport coefficients, and (iv) numerical method is described below.

2.1. Equations of fluid motion

The turbulent flow motion of supercritical fluids is described by the following set of conservation equations of mass, momentum, and total energy

$$\frac{\partial \rho}{\partial t} + \nabla \cdot (\rho \mathbf{v}) = 0, \tag{1}$$

$$\frac{\partial (\rho \mathbf{v})}{\partial t} + \nabla \cdot (\rho \mathbf{v} \mathbf{v}) = -\nabla P + \nabla \cdot \boldsymbol{\tau}, \tag{2}$$

$$\frac{\partial (\rho E)}{\partial t} + \nabla \cdot (\rho \mathbf{v} E) = -\nabla \cdot \mathbf{q} - \nabla \cdot (P \mathbf{v}) + \nabla \cdot (\boldsymbol{\tau} \cdot \mathbf{v}), \tag{3}$$

where ρ is the density, $\mathbf{v}$ is the velocity vector, P is the pressure, $\boldsymbol{\tau} = \mu \left(\nabla \mathbf{v} + \nabla \mathbf{v}^T \right) - (2\mu/3)(\nabla \cdot \mathbf{v})\boldsymbol{I}$ is the viscous stress tensor with μ the dynamic viscosity and $\boldsymbol{I}$ the identity matrix, E is the total energy, $\mathbf{q} = -\kappa \nabla T$ is the Fourier heat flux with κ is the thermal conductivity.

2.2. Real-gas thermodynamics

The thermodynamic space of solutions for the state variables pressure P, temperature T, and density ρ of a single substance is described by an equation of state. One popular

7

109 choice for systems at high pressures, which is used in this study, is the Peng-Robinson [14]
110 equation of state written as

$$P = \frac{R_u T}{\bar{v} - b} - \frac{a}{\bar{v}^2 + 2b\bar{v} - b^2}, \tag{4}$$

with R_u the universal gas constant, $\bar{v} = W/\rho$ the molar volume, and W the molecular weight. The coefficients a and b take into account real-gas effects related to attractive forces and finite packing volume, respectively, and depend on the critical temperature T_c, critical pressure P_c, and acentric factor ω. They are defined as

$$a = 0.457 \frac{(\mathrm{R_u} T_c)^2}{P_c} \left[1 + c \left(1 - \sqrt{T/T_c} \right) \right]^2, \tag{5}$$

$$b = 0.078 \frac{\mathrm{R_u} T_c}{P_c}, \tag{6}$$

where coefficient c is provided by

$$c = \begin{cases} 0.380 + 1.485\omega - 0.164\omega^2 + 0.017\omega^3 & \text{if } \omega > 0.49, \\ 0.375 + 1.542\omega - 0.270\omega^2 & \text{otherwise.} \end{cases} \tag{7}$$

111 The Peng-Robinson real-gas equation of state needs to be supplemented with the
112 corresponding high-pressure thermodynamic variables based on departure functions [15]
113 calculated as a difference between two states. In particular, their usefulness is to trans-
114 form thermodynamic variables from ideal-gas conditions (low pressure - only temperature
115 dependant) to supercritical conditions (high pressure). The ideal-gas parts are calculated
116 by means of the NASA 7-coefficient polynomial [16], while the analytical departure expres-
117 sions to high pressures are derived from the Peng-Robinson equation of state as detailed,
118 for example, in Jofre & Urzay [2].

2.3. High-pressure transport coefficients

120 The high pressures involved in the analyses conducted in this work prevent the use of
121 simple relations for the calculation of the dynamic viscosity μ and thermal conductivity κ.
122 In this regard, standard methods for computing these coefficients for Newtonian fluids are
123 based on the correlation expressions proposed by Chung et al. [17, 18]. These correlation
124 expressions are mainly function of critical temperature T_c and density ρ_c, molecular weight

8

125 W, acentric factor ω, association factor κ_a and dipole moment $\mathcal{M}$, and the NASA 7-
126 coefficient polynomial [16]; further details can be found in dedicated works, like for example
127 Poling et al. [19] and Jofre & Urzay [2].

2.4. Numerical method

129 The equations of fluid motion introduced in Section 2.1 are numerically solved by
130 adopting a standard semi-discretization procedure; viz. they are firstly discretized in
131 space and then integrated in time. In particular, spatial operators are treated using
132 second-order central-differencing schemes, and time-advancement is performed by means
133 of a third-order strong-stability preserving (SSP) Runge-Kutta explicit approach [20].
134 The convective terms are expanded according to the Kennedy-Gruber-Pirozzoli (KGP)
135 splitting [21, 22], which has been recently assessed for high-pressure supercritical fluids
136 turbulence [23, 24]. The method preserves kinetic energy by convection, and is locally
137 conservative for mass, momentum, and total energy. This numerical framework provides
138 stable computations without the need of any form of artificial dissipation or stabilization
139 procedures.

3. Data-driven dimensional analysis

141 In this section, the integration of classical dimensional analysis with modern dimension
142 reduction techniques is described. The resulting tools enable data-driven discovery of
143 unique and relevant dimensionless groups in multiphysics turbulent flow problems [13].

3.1. Dimensional analysis and the π subspace

145 Prior to directly diving into the theoretical basis of dimensional analysis, it is useful
146 to provide some initial notation. In this regard, the *dimension function* of a quantity q,
147 referred to as $[q]$, is defined as a function that returns the dimension of q in terms of the
148 base units: length L [m], mass M [kg], time T [s], temperature θ [K]; e.g., if q is velocity,
149 then $[q]$ is L/T. Accordingly, the *dimension vector* of a quantity q, denoted $\mathbf{v}(q)$, is defined
150 as a function that returns the k exponents of $[q]$ with respect to the dimensions of the

base units. For example, in a system with $k = 3$ dimensions L, M and T, if q is velocity, then $[q] = L^1 \cdot M^0 \cdot T^{-1}$ and $\mathbf{v}(q) = [1, 0, -1]^\top$.

Dimensional analysis is a classical dimension reduction technique. Its central result is the Buckingham's π theorem [9], which states that given a set of dimensional inputs $\mathbf{q} \in \mathbb{R}^m$ that predict a dimensionless QoI, i.e., $Q = f(\mathbf{q})$, the functional relationship may be re-expressed in terms of a smaller number of dimensionless numbers $\boldsymbol{\pi} \in \mathbb{R}^n$ via $\pi_i = \psi(\pi_1, \ldots, \pi_n)$. The set of dimensionless inputs $\boldsymbol{\pi} = \{\pi_1, \ldots, \pi_n\}$ can be determined from the dimension matrix $\mathbf{D} \in \mathbb{R}^{k \times m}$ of rank k, which is given for $\mathbf{q}$ as [11]

$$\mathbf{D} = [\mathbf{v}(q_1), \ldots, \mathbf{v}(q_m)]. \tag{8}$$

Valid dimensionless numbers can be formed by products of the inputs as [11]

$$\pi_i = \prod_{j=1}^{m} q_i^{z_{ij}}, \tag{9}$$

with the vectors $\{\mathbf{z}_i\}_{i=1}^n$ satisfying $\mathbf{D}\mathbf{z}_i = \mathbf{0}_{k \times 1}$. In this formulation, the Buckingham's π theorem can be understood in terms of the rank-nullity theorem, which states that the number of independent dimensionless groups is given by $n = \dim[\mathcal{R}(\mathbf{D})] - \dim[\mathcal{N}(\mathbf{D})]$, where $\dim[\cdot]$ is the subspace dimension, $\mathcal{R}(\cdot)$ denotes the range, and $\mathcal{N}(\cdot)$ denotes the nullspace. The Buckingham's π theorem is silent on the choice of a basis for the nullspace of $\mathbf{D}$, i.e., $\{\mathbf{z}_i\}_{i=i}^n$. In this regard, since the dimensionless groups depend on the choice of this basis, they are not unique and often selected based on experience. Instead, in this work data will be used to inform a useful selection of relevant $\boldsymbol{\pi}$ groups.

3.2. Active subspaces and dimensional analysis

The active subspace is a dimension reduction concept introduced by Russi [25] and developed by Constantine [26]. Let $f(\mathbf{x})$ be some differentiable QoI on a domain with integral weight $\rho(\mathbf{x}) \in \mathbb{R} \geq 0$. The active subspace is then defined in terms of the matrix

$$\mathbf{C} \equiv \int \nabla_{\mathbf{x}} f \nabla_{\mathbf{x}} f^\top \rho(\mathbf{x}) d\mathbf{x}. \tag{10}$$

Since $\mathbf{C}$ is by construction symmetric semi-positive definite, it admits an eigenvalue decomposition of the form $\mathbf{C} = \mathbf{U}\boldsymbol{\Lambda}\mathbf{U}^\top$. The eigenvalues need to be sorted first in decreasing

order as $\lambda_1 \geq \cdots \geq \lambda_n$. Next, a threshold separating $\{\lambda_1, \ldots, \lambda_n\}$ into large $\{\lambda_1, \ldots, \lambda_A\}$ and small $\{\lambda_{A+1}, \ldots, \lambda_n\}$ eigenvalues is defined to generate the split $\mathbf{U} = [\mathbf{U}_A, \mathbf{U}_I]$. The final result is that the directions $\mathbf{u}_i$ are then ordered in decreasing order of importance with respect to variation in the QoI f, made quantitative by the eigenvalues, which is equivalent to the mean-squared directional derivative along direction $\mathbf{u}_i$. The active subspace is then given by $\mathcal{R}(\mathbf{U}_A)$, where the columns of $\mathbf{U}_A$ form a basis for the subspace. Furthermore, using the vector entries in Eq. (9), the active directions $\mathbf{u}_{A,i}$ can be directly interpreted as dimensionless groups.

3.3. Dimensionality reduction methodology

The methodology starts by considering a physical system with $m + 1$ dimensional quantities Q and $\mathbf{q} = [q_1, \ldots, q_m]^\top$, whose units are derived from a set of k base units satisfying $m > k$. Without loss of generality, it is assumed that Q is the quantity of interest, while $\mathbf{q}$ are the independent variables. By considering the corresponding $\mathbf{D}$ matrix of rank k, it can be then constructed a dimensionless independent variable $\pi = \pi(Q, \mathbf{q}) = Q \exp\left[-\mathbf{w}^\top \log(\mathbf{q})\right]$, where the exponents $\mathbf{w}$ satisfy the linear system $\mathbf{D}\mathbf{w} = \mathbf{v}(Q)$. The solution $\mathbf{w}$ is not unique since $\mathbf{D}$ has a nontrivial nullspace. In this regard, let $\mathbf{W} = [\mathbf{w}_1, \ldots, \mathbf{w}_n] \in \mathbb{R}^{m \times n}$ be a matrix whose columns contain a basis for the nullspace of $\mathbf{D}$, i.e., $\mathbf{D}\mathbf{W} = \mathbf{0}_{k \times n}$, where each column of $\mathbf{W}$ represents a dimensionless group. Then, given pairs $[\mathbf{q}^{(1)}, Q^{(1)}], \ldots, [\mathbf{q}^{(N)}, Q^{(N)}]$ from a design of experiment with N samples consistent with the joint probability density $\rho(\mathbf{q})$, the data-driven dimensional analysis methodology is composed of the following steps: (1) compute evaluations of the dimensionless independent variable $\pi^{(j)} = Q^{(j)} \exp\{-\mathbf{w}^\top \log\left[(\mathbf{q}^{(j)}\right]\}$ with $j = 1, \ldots, N$; (2) calculate logs of the dimensionless groups as $\gamma_i^{(j)} = \mathbf{w}_i^\top \log\left[\mathbf{q}^{(j)}\right]$ with $i = 1, \ldots, n$ and $\boldsymbol{\gamma}^{(j)} = \left[\gamma_1^{(j)}, \ldots, \gamma_n^{(j)}\right]^\top$; (3) fit a response surface g with the pairs $\{\left[\pi^{(j)}, \boldsymbol{\gamma}^{(j)}\right]\}$ such that $\pi^{(j)} \approx g\left[\boldsymbol{\gamma}^{(j)}\right]$ with $j = 1, \ldots, N$; (4) use the response surface gradient ∇g to approximate active subspaces $\mathbf{C} = \int \nabla g(\boldsymbol{\gamma}) \nabla g(\boldsymbol{\gamma})^\top \rho(\boldsymbol{\gamma}) d\boldsymbol{\gamma} \approx \mathbf{U}\boldsymbol{\Lambda}\mathbf{U}^\top$; and (5) compute the weights vectors $\mathbf{z}_i = \mathbf{W}\mathbf{u}_i$ that define the unique and relevant dimensionless groups $\pi_i = q_1^{z_{i,1}} \times \cdots \times q_m^{z_{i,m}}$ with $i = 1, \ldots, n$. It is important to note that the singular values $\boldsymbol{\Lambda}$ provide a measure of the relative importance between the π groups obtained.
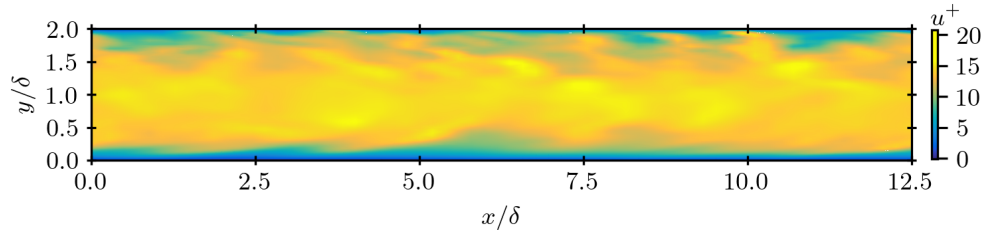
11

Figure 1: Snapshot of instantaneous streamwise velocity in wall units u^+ on a x-y slice.

4. Generation of synthetic data

The setup of the problem is designed to study non-buoyant microconfined high-pressure supercritical fluid turbulence at transcritical conditions. As illustrated in Figure 1, the analysis of such systems involves the interaction of microfluidics, thermodynamics and turbulence. The instantaneous snapshot, extracted from a direct numerical simulation (DNS), corresponds to the streamwise velocity in wall units u^+ on a x-y slice. A complete description of the problem setup and system parameters is presented in the subsections below.

4.1. Problem setup

The channel flow problem is a reference experiment widely used in the computational fluid dynamics community to validate and analyze wall-bounded turbulent flows. In this regard, the channel flow setup is chosen to study and characterize high-pressure supercritical fluids turbulence at the microscale. In particular, by means of slightly perturbing the values of molecular weight W and acentric factor ω, the fluid selected as a reference substance to generate different "artificial" fluids is N_2 whose critical pressure and temperature are $P_c = 3.4\,\text{MPa}$ and $T_c = 126.2\,\text{K}$, respectively. The fluid system is at a supercritical bulk (i.e., ensemble-averaged) pressure of P_b and confined between cold/bottom (cw) and hot/top (hw) isothermal walls, separated at a hydraulic diameter $D_h \approx 2\delta$ with δ the channel half-height, at $T_{cw} = 100\,\text{K}$ and T_{hw} below and above, respectively, the pseudo-boiling temperature at the corresponding bulk pressure and resulting in an imposed temperature difference $\Delta T_w = T_{hw} - T_{cw}$ between walls. This problem setup imposes the fluid to undergo a transcritical trajectory by operating within a thermodynamic

12

region across the pseudo-boiling line. In addition, as studied by Bernades et al. [3, 5, 6], the bulk velocity u_b in Table 1 has been selected to attain turbulent flow conditions. The mass flow rate in the streamwise direction is imposed through a body force controlled by a feedback loop to achieve the desired bulk velocity values. In addition, gravity forces are not considered as the resulting Froude number of the problem is $Fr = u_b/\sqrt{gD_h} \approx 23$, and consequently inertial forces are roughly $530\times$ more important than gravitational effects; viz. the importance of gravity scales as $1/Fr^2$.

As schematically represented in Figure 2, the computational domain is $4\pi\delta \times 2\delta \times (4/3)\pi\delta$ in the streamwise (x), wall-normal (y), and spanwise (z) directions, respectively, which is large enough to represent the largest flow scales of the problem [27]. The streamwise and spanwise boundaries are set periodic, and no-slip conditions are imposed on the horizontal boundaries (x-z planes). The mesh resolution is selected based on preliminary studies. In particular, the fine-resolved DNS of turbulent channel flow performed by Chevalier et al. [28] at a similar Re_b, which utilized $64 \times 64 \times 64$ grid points, is considered as an initial reference. For the problem of interest in this work, in addition to the classical consideration of the Kolmogorov and boundary layer scales, the length scales related to density gradients must also be considered. To this extent, based on the estimations provided by Jofre & Urzay [1], the characteristic length scale for density gradients is approximately $10\times$ larger than the Kolmogorov scale, thereby confirming that the latter is the driving factor to select mesh resolution. Nonetheless, the mesh selected is $2\times$ finer in each direction with respect to Chevalier et al. [28]. Consequently, this grid arrangement corresponds to a DNS of size $128 \times 128 \times 128$ grid points. The grid is uniform in the streamwise and spanwise directions with resolutions in wall units (based on cw values) equal to $\Delta x^+ \approx 9.8$ and $\Delta z^+ \approx 3.3$, and stretched toward the walls in the vertical direction with the first grid point at $y^+ = yu_{\tau,cw}/\nu_{cw} \approx 0.1$ and with sizes in the range $0.2 \lesssim \Delta y^+ \lesssim 2.3$. The simulation strategy starts from a linear velocity profile with random fluctuations, which is advanced in time to reach turbulent steady-state conditions after approximately 5 flow-through-time (FTT) units and collect flow statistics for roughly 10 FTTs once steady-state conditions are achieved.

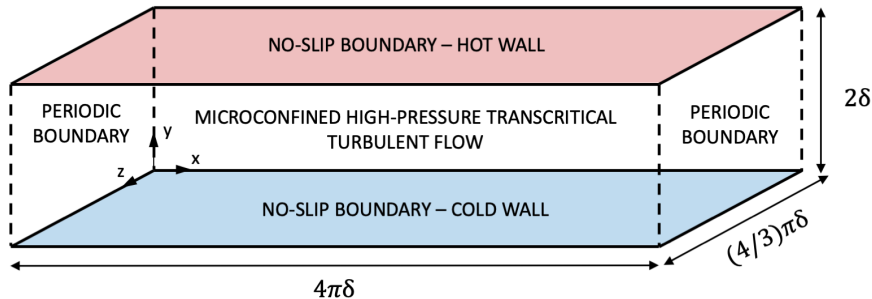Figure 2: Schematic illustration of the microconfined channel flow computational setup.

Parameter	Value	Parameter	Value
P_b	$[3.75 : 6.25]$ MPa	D_h	$[150 : 250]$ μm
u_b	$[1.5 : 2.5]$ m/s	W	$[22.5 : 37.5]$ g/mol
ΔT_w	$[75 : 125]$ K	ω	$[0.0225 : 0.0375]$

Table 1: List of system parameters and their range of values.

4.2. System parameters

The study conducted in this work is designed with the objective of mimicking an experiment as it would be carried out in a laboratory facility. The system is characterized by the 6 parameters listed in Table 1 that can be varied independently to collect data. The ranges of these values are obtained by adding/subtracting 25% to/from their nominal values as these are parameters that in a laboratory facility would not be easily modified in significantly large proportions. It is important to note that the principle of corresponding states [viz. all fluids, when compared at the same $T_r = T/T_c$ and $P_r = P/P_c$, have (i) approximately the same compressibility factor Z and (ii) all deviate similarly from ideal gas] enables to discard critical pressure P_c, critical temperature T_c and critical molar volume $\bar{v}_c$ as independent parameters since effects can be accounted through varying bulk pressure P_b and bulk temperature T_b. Moreover, a third corresponding-states parameter [29], the acentric factor ω, provides a measure of the non-sphericity of the force field of a molecule. On the contrary, the dipole moment, which is a measure of the polarity of the molecule, is assumed to be zero for the fluids considered. In terms of the data-driven

dimensional analysis, the set of system parameters listed in Table 1 are transformed, through the thermophysical models presented in Section 2 and the bulk values of the computational data obtained from the simulations, to the following 8 dimensional inputs (P_b and ω accounted through thermophysical quantities): hydraulic diameter D_h [m], bulk velocity u_b [m/s], bulk temperature T_b [K], specific gas constant R' [J/(kg · K)], bulk density ρ_b [kg/m³], bulk dynamic viscosity μ_b [Pa · s], bulk thermal conductivity κ_b [W/(m · K)], and bulk isobaric specific heat capacity c_{P_b} [J/(kg · K)]. Data are collected by computing 48 DNS using the in-house flow solver RHEA [30] of the problem for different values of the system parameters following a design of experiment based on a Latin hypercube sampling (LHS) approach [31].

5. Results and discussion

This section analyzes the data acquired by computing the set of samples described in Section 4 based on the physics modeling presented in Section 2, and provides a characterization of the flow and discussion of the results obtained from the methodology introduced in Section 3.

5.1. Flow physics characterization

The purpose of this subsection is to briefly characterize the flow physics of the ensemble of samples based on first- and second-order statistics; complete analyses of the flow physics of non-buoyant microconfined high-pressure supercritical fluid turbulence is reported in Bernades et al. [5, 6]. The results are displayed in terms of (i) the mean profile of the distributions, and (ii) the envelope of all samples. Particularly, Fig. 3(a) shows the normalized profile of time-averaged streamwise velocity $\tilde{u}/u_b$ as a function of distance to the wall y/D_h, whereas Fig. 3(b) depicts the normalized turbulent kinetic energy (TKE) k/u_b^2. Based on the results presented in these two plots, it can be seen that the profiles exhibit the typical characteristics of turbulent flow: (i) power-law-like shape for the time-averaged streamwise velocity, which is indicative of a viscous-dominated region close to a solid boundary that rapidly transitions to a logarithmic behavior away from it; and (ii) high levels of TKE in the near-wall regions resulting from the large velocity gradients

15

generated by friction (peak values within the buffer layer). It is also important to note that, due to the asymmetric temperature distribution in the wall-normal direction (viz. liquid-like supercritical fluid presents larger inertia than gas-like supercritical fluid), the profiles are not exactly symmetric across the channel centerline. In addition, as illustrated by the size of the envelopes with respect to the mean profiles, the samples present relevant levels of variability across them, with maximum coefficients of variation CoV $\approx 12\%$ and CoV $\approx 8\%$ for $\tilde{u}/u_b$ and k/u_b^2, respectively.

Focusing on the normalized time-averaged temperature difference $(\tilde{T} - T_{cw})/T_b$ and Favre-averaged temperature fluctuations T''/T_b depicted in Fig. 3(c) and Fig. 3(d), three main results can be observed. First, the time-averaged temperature difference monotonically increases from the cold to the hot wall, presenting a notably rapid variation in the vicinity of the hot wall. Second, the Favre-averaged temperature fluctuations increase following a similar trajectory, but exhibiting a significantly large peak in the buffer layer of the hot wall. These two observations, as explained in detail by Bernades et al. [5, 6], are connected and attributed to the presence of the pseudo-boiling line across which the fluid transitions from supercritical liquid-like to supercritical gas-like. Finally, third, the profiles are virtually horizontal through the centerline section of the channel, indicating that the fluid is highly mixed in that region. It is important to highlight that the samples present also relevant levels of variability across them in terms of temperature, with maximum coefficients of variation CoV $\approx 13\%$ and CoV $\approx 13\%$ for $(\tilde{T} - T_{cw})/T_b$ and T''/T_b, respectively.

5.2. Data-driven inference of principal π groups

Focusing on the normalized bulk specific turbulent kinetic energy (spatial-ensemble average of 10 FTTs) $k = (u''^2 + v''^2 + w''^2)/2$, with superscript $''$ indicating Favre-averaged fluctuations, as a quantity of interest, i.e., $Q \equiv k_b/u_b^2$, which is a measure of the turbulent intensity of the system, the data-driven dimensional analysis strategy described in Section 3 is utilized to infer principal dimensionless groups from the data collected. As discussed in Section 4, the problem of interest considers $m = 8$ dimensional inputs (D_h, u_b, T_b, R', ρ_b, μ_b, κ_b, c_{P_b}) with $k = 4$ base units (L, M, T, θ), which based on the Buckingham's π theorem results in $n = m - k = 4$ dimensionless groups. However, as
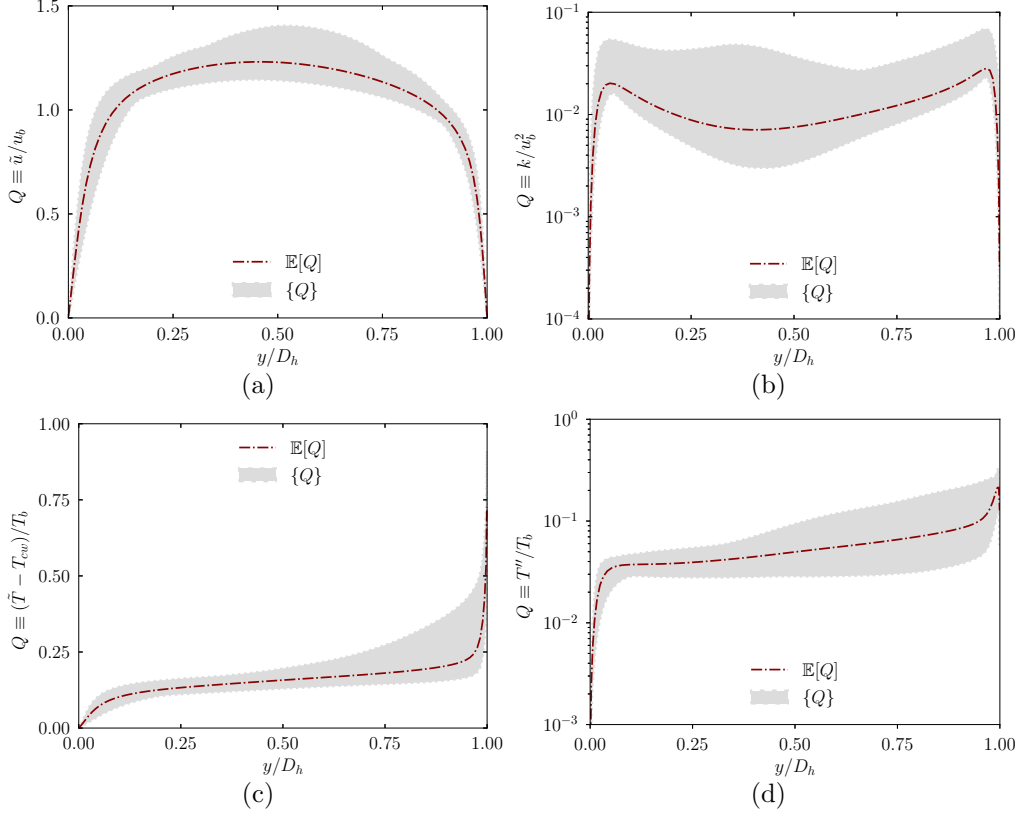
16

Figure 3: Normalized profiles along the wall-normal direction y/D_h of time-averaged streamwise velocity $\tilde{u}/u_b$ (a), turbulent kinetic energy k/u_b^2 (b), time-averaged temperature difference $(\tilde{T} - T_{cw})/T_b$ (c), and Favre-averaged temperature fluctuations T''/T_b (d). Dashed-dotted lines correspond to the mean of the distributions, and filled regions show the envelope of all samples.

Group	D_h	u_b	T_b	R'	ρ_b	μ_b	κ_b	c_{P_b}	σ_i/σ_1
π_1	0.20	0.40	-0.10	-0.46	0.20	-0.61	0.41	-0.05	1.00
π_2	0.46	-0.33	0.39	0.41	0.46	-0.37	-0.09	0.07	0.06
π_3	0.29	0.55	-0.13	-0.05	0.29	0.23	-0.52	0.43	0.02
π_4	-0.05	-0.45	0.20	-0.53	-0.05	0.01	0.04	0.69	0.01

Table 2: Exponents z_{ij} of the dimensional inputs defining the data-driven inferred dimensionless groups π_i, together with the corresponding normalized singular values σ_i/σ_1.

previously stated, this theorem does not indicate (i) which are the dimensionless numbers to consider, neither (ii) the relative importance between them.

Following the methodology presented in Section 3, the exponents z_{ij} of Eq. (9) defining the 4 dimensionless groups π_i inferred from data are provided in Table 2, together with the corresponding singular values normalized with respect to the first eigenvector, i.e., σ_i/σ_1; the values have been rounded to 2 significant digits, and consequently may not exactly provide dimensionless units. Prior to analyzing their composition, it is important to note that π_1 (first dimensionless group) is approximately $18\times$, $47\times$ and $79\times$ more important, based on the corresponding singular values, than π_2, π_3 and π_4, respectively. In this regard, the analysis is focused on the first dimensionless group written in terms of the dimensional inputs as

$$\pi_1 \approx D_h^{0.20} \times u_b^{0.40} \times T_b^{-0.10} \times R'^{-0.46} \times \rho_b^{0.20} \times \mu_b^{-0.61} \times \kappa_b^{0.41} \times c_{P_b}^{-0.05}. \qquad (11)$$

The expression above enables to plot the quantity of interest k_b/u_b^2 as a function of the first dimensionless group π_1 inferred. The result is plotted in Figure 4(a) for the 48 samples considered in this study. The plot clearly depicts a significantly high degree of data collapse with respect to π_1, and consequently demonstrates the effectiveness of the methodology proposed to infer unique and relevant dimensionless groups. In particular, the normalized bulk turbulent kinetic energy tends to decrease as π_1 increases; viz. k_b increases with π_1, but less rapidly than u_b^2, and as a result k_b/u_b^2 tends to decrease. A more insightful, and easier to interpret, dimensionless group is derived and discussed in
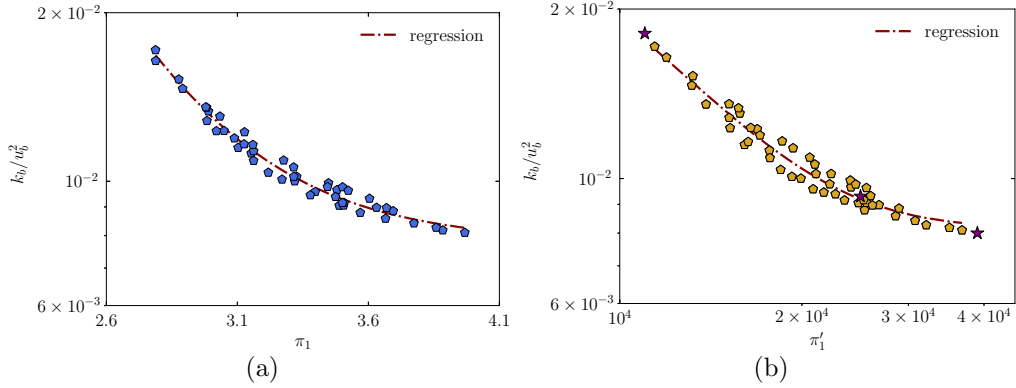
Figure 4: Normalized bulk turbulent kinetic energy k_b/u_b^2 for the 48 samples plotted as a function of the inferred π_1 (a) and proposed (simplified) π_1' (b) dimensionless groups. Dashed-dotted lines correspond to nonlinear regression curves of the data, while the purple stars represent three additional cases computed to test the quality of the fitness.

the next subsection.

5.3. Interpretation in terms of standard dimensionless numbers

The data-driven methodology described in Section 3 allows one to easily re-express the π_i groups as powers of standard dimensionless numbers $\hat{\pi}_i$ through a simple linear algebra transformation. In detail, provided the matrix $\mathbf{V} \in \mathbb{R}^{m \times k}$ describing the weights of the dimensional inputs defining the basis for the standard dimensionless numbers selected, the solution, for example through a least squares approximation, to the inverse problem $\mathbf{V}\mathbf{s}_i = \mathbf{z}_i$ with $i = 1, \ldots, n$ enables to re-express the dimensional groups inferred in terms of standard dimensionless numbers by the weight vectors $\mathbf{s}_i$ as [11]

$$\pi_i = \prod_{j=1}^{n} \hat{\pi}_i^{s_{ij}}. \tag{12}$$

As a basis for re-expressing the π_i groups, widely recognized dimensionless numbers in fluid mechanics resulting from normalizing the equations and boundary conditions describing the problem are utilized. Their definitions are given in Table 3, where the speed of sound has been approximated for real gases to sos $\approx \sqrt{\hat{\gamma} R' T}$, with $\hat{\gamma}$ the approximated

19

Dimensionless number	Definition
Fluid & flow groups:	
Bulk Reynolds number	$Re_b = \rho_b u_b D_h / \mu_b$
Bulk Prandtl number	$Pr_b = c_{P_b} \mu_b / \kappa_b$
Bulk Eckert number	$Ec_b = u_b^2 / (c_{p_b} T_b)$
Bulk Mach number	$Ma_b = u_b / c_b$
Factors & ratios:	
Compressibility factor	$Z = P / (\rho R' T)$
Real-gas heat capacity ratio	$\hat{\gamma} \approx Z c_P / (c_P - Z R')$

Table 3: List of standard fluid mechanics dimensionless numbers and parameters for the system of interest obtained from the equations of fluid motion. Subindexes b and w indicate, respectively, bulk and wall values.

real-gas heat capacity ratio [32] defined in the same table. Particularly, the standard dimensionless groups correspond to: (i) Reynolds number Re quantifying the ratio of inertial to viscous forces; (ii) Prandtl number Pr assessing the ratio of momentum to thermal diffusivity; (iii) Eckert number Ec accounting for the ratio between advective mass transfer and heat dissipation potential, and (iv) Mach number Ma indicating the ratio between flow velocity and speed of sound. Hereof, to highlight the importance of inferring unique and relevant dimensionless groups in contrast to directly utilizing the standard dimensionless numbers selected, Figure 5 depicts the quantity of interest k_b / u_b^2 as a function of Re_b (a), Pr_b (b), Ec_b (c) and Ma_b (d) for the 48 samples computed. The plots indicate that the data tends to mildly collapse to a curve for Re_b (especially), Ec_b and Ma_b, but not for Pr_b. In addition, there is no straightforward route to quantify the relative importance between these dimensionless numbers.

Utilizing the set of dimensionless numbers listed in Table 3 as the transformation basis, the π_i dimensionless groups inferred from data in the previous subsection can be re-expressed as products of standard fluid mechanics groups. The decomposition for the
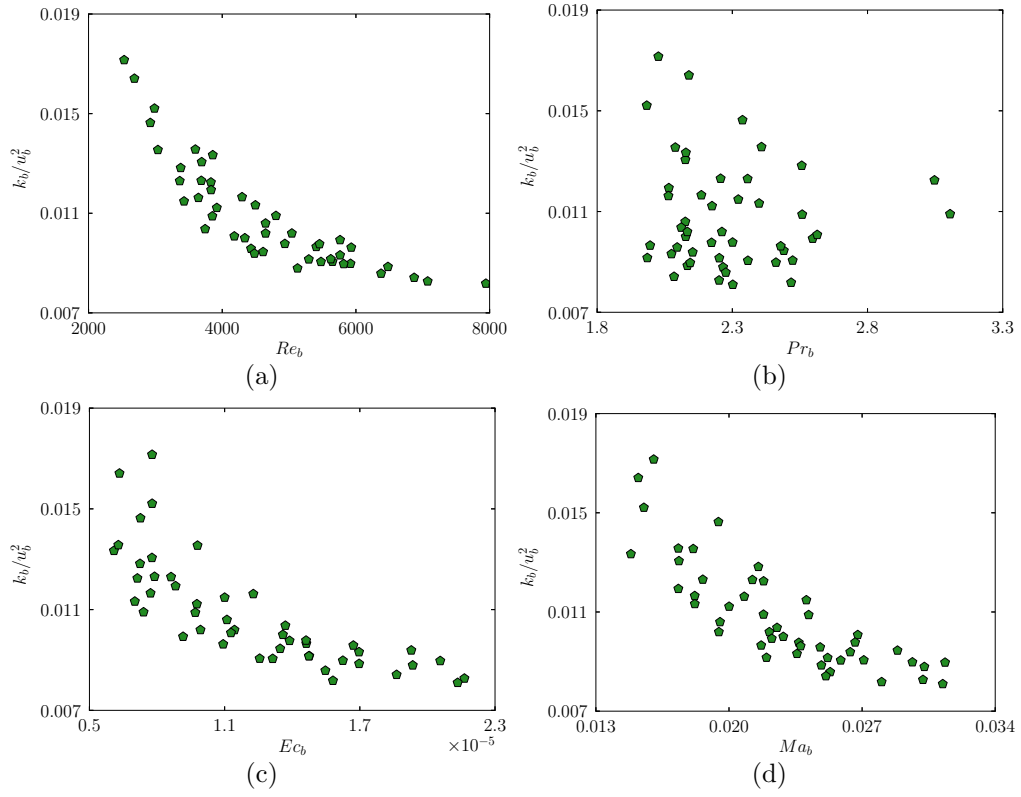
Figure 5: Normalized bulk turbulent kinetic energy k_b/u_b^2 for the 48 samples plotted as a function of the standard dimensionless numbers Re_b (a), Pr_b (b), Ec_b (c) and Ma_b (d).

first (most important) dimensionless group corresponds to

$$\pi_1 \approx Re_b^{0.20} \times Pr_b^{-0.41} \times Ec_b^{-0.36} \times Ma_b^{0.92}, \tag{13}$$

where the exponent weights have been rounded to 2 significant digits, and as a result may not exactly provide dimensionless quantities. The structure of the dimensionless group in terms of the standard dimensionless numbers indicates that (i) it sublinearly scales with Re_b and Ma_b, and (ii) is inversely proportional to Pr_b and Ec_b. Further analyses in terms of sensitivities and physical insight are discussed in the next subsection.

5.4. Derivation of a simplified new dimensionless group

The final objective of this work is to derive a simplified new dimensionless group describing the amount of turbulent kinetic energy in non-buoyant microconfined high-pressure supercritical fluid turbulence. The first step is to calculate the sensitivities of the quantity of interest Q with respect to the dimensional inputs $\mathbf{q}$ through the inferred dimensional group π_1. To that end and based on the results obtained in Section 5.2, the quantity of interest $Q = Q(\pi_1, \pi_2, \pi_3, \pi_4)$ is approximated to $\tilde{Q} = \tilde{Q}(\pi_1)$ since the first dimensionless group π_1 is significantly more important than the other ones. Then, the sensitivities can be calculated for $j = 1, \ldots, m$ as

$$\left. \frac{\partial \tilde{Q}}{\partial q_j} \right|_{q_{k|k \neq j}} = \frac{d\tilde{Q}}{d\pi_1} \cdot \left. \frac{\partial \pi_1}{\partial q_j} \right|_{q_{k|k \neq j}}, \tag{14}$$

which are later normalized multiplying each one by the corresponding mean q_j value to compare the relative importance between them, and where $d\tilde{Q}/d\pi_1$ is constant for all $\mathbf{q}$. In this regard, the values of the normalized $(\partial \pi_1 / \partial q_j) \cdot \mathbb{E}[q_j]$ sensitivities are: 0.66 for D_h, 1.37 for u_b, -0.35 for T_b, -1.58 for R', 0.66 for ρ_b, -2.03 for μ_b, 1.39 for κ_b, and -0.18 for c_{P_b}. Notice that the larger (absolute value) sensitivities are related to D_h, u_b, R', ρ_b, μ_b and κ_b. As a result, the following simplified new dimensionless number is proposed

$$\pi_1' = \frac{\rho_b u_b D_h \kappa_b}{\mu_b^2 R'} = \frac{Re_b c_{Pb}}{Pr_b R'}, \tag{15}$$

which presents the structure of an augmented Reynolds number $Re_b = \rho_b u_b D_h / \mu_b$ accounting for thermophysical effects through κ_b, μ_b and R', or equivalently Pr_b, c_{Pb} and

22

R'. In this regard, the quantity of interest k_b/u_b^2 is plotted as a function of this new proposed dimensionless number π_1' in Figure 4(b), which demonstrates that π_1' efficiently describes the level of turbulent kinetic energy in non-buoyant microconfined high-pressure supercritical fluid turbulence by collapsing the data from the 48 samples into a (roughly) single curve as illustrated by the nonlinear regression. It is important to note that for a given c_{Pb} and R', the relation between Re_b and normalized TKE depends on the value of Pr_b as: (i) the importance of heat diffusion is reduced for large Prandtl values (corresponding to small π_1' values), and as a result convective motions dominate the flow resulting in relatively high levels of normalized TKE; on the contrary, (ii) for small Prandtl numbers (corresponding to large π_1' values), in which heat diffusion becomes important, diffusion effects dominate the system and, as a result, turbulent fluctuations are reduced.

The performance in collapsing the data of the simplified dimensionless group π_1' with respect to the directly inferred dimensionless group π_1 can be quantified based on the coefficient of determination (CoD). The CoD, typically denoted as R^2, provides a measure of how well observed outcomes are replicated by a model relative to the proportion of total variation of outcomes explained by it. Therefore, given a dataset of $n = 48$ values $y_1, \ldots y_n$, each associated with a fitted, or modeled/predicted, value $f_1, \ldots f_n$ from which a residual $e_i = y_i - f_i$ can be computed, the mathematical definition of R^2 is written as [33]

$$R^2 \equiv 1 - \frac{SS_{\text{res}}}{SS_{\text{tot}}}, \tag{16}$$

where $SS_{\text{res}} = \sum_{i=1}^{n}(y_i - f_i)^2 = \sum_{i=1}^{n} e_i^2$ is the residual sum of squares, and $SS_{\text{tot}} = \sum_{i=1}^{n}(y_i - \bar{y})^2$ is the total sum of squares (proportional to the variance of the data) with $\bar{y} = n^{-1}\sum_{i=1}^{n} y_i$ the mean of the observed data. In this regard, based on the nonlinear regression curves shown in Figure 4 representing the fitted values $f_1, \ldots f_n$, the CoD values correspond to $R^2 \approx 0.98$ and $R^2 \approx 0.96$ for π_1 and π_1', respectively. As it can be seen, both CoDs are relatively high, which is indicative of good data collapse, and presenting a slight difference of only 2%. Consequently, π_1' is a good approximation of π_1. Finally, to further verify the quality of the fitness, three additional cases for $\pi_1' \approx$ 11000 (low), 25000 (medium), 39000 (high) have been computed and added to Figure 4(b) as purple stars. As it can be noted from the plot, these additional cases lie within the

23

spread of the data, and consequently reinforce the capability of π_1' to collapse the data into a single curve.

6. Conclusions

Multiphysics flow problems, such as high-pressure supercritical fluids turbulence, (typically) involve the analysis of complex high-dimensional parameter spaces. Their study can be systematically approached by considering important dimensionless groups characterizing the underlying physics phenomena, which, in addition to reducing the dimensionality of the system, provide notable support for the inference of similarity laws and a basis for out-of-scale modeling. However, classical dimensional analysis techniques present two main shortfalls as the set of scale-free groups are not unique, and there is no general methodology for quantifying their relative importance and physically interpreting the results. This work, therefore, has leveraged a novel data-driven methodology aimed to address these deficiencies by augmenting Buckingham's π theorem with ideas developed in the field of active subspaces tailored to the study of complex turbulent flow applications.

The data-driven methodology presented has been utilized to infer important dimensionless groups of the problem at high-pressure transcritical thermodynamic regimes close to the critical point. In particular, a principal dimensionless group has been identified that is able to efficiently describe the behavior of the system in terms of normalized bulk turbulent kinetic energy. Its decomposition in terms of standard fluid mechanics dimensionless numbers indicates that (i) it sublinearly scales with Re_b and Ma_b, and (ii) is inversely proportional to Pr_b and Ec_b. In addition, based on the normalized sensitivities of the quantity of interest to the dimensional inputs, a corresponding simplified novel dimensionless group has been proposed of the form $\pi_1' = \rho_b u_b D_h \kappa_b / (\mu_b^2 R')$. It presents the structure of an augmented Reynolds number accounting for thermophysical effects through dynamic viscosity, thermal conductivity and specific gas constant, and is able to efficiently describe the level of turbulent kinetic energy in non-buoyant microconfined high-pressure supercritical fluid turbulence by collapsing the data into a (roughly) single curve. Finally, the input parameter space selected for this study has been designed based on realistic regimes inspired by Nitrogen at microfluidic conditions. Consequently, the results obtained can be

24

generalized to other fluids, like for example CO_2, CH_4, O_2, R134a and H_2O, by means of the principle of corresponding states.

Ongoing work is concentrated on corroborating experimentally the performance of the novel dimensionless group inferred by carrying out microconfined laboratory tests at high-pressure transcritical operating conditions. Future work will focus on expanding the data-driven methodology to (i) generate simplified decompositions of the dimensionless groups inferred by means of L1-regularization (Lasso regression) approaches, and (ii) generalize it to simultaneously treat different quantities of interest. In addition, wider ranges of the external parameters of the problem of interest will be analyzed to further corroborate the scientific findings described in this work, and to carry out studies for the engineering optimization of energy transfer in microconfined systems based on high-pressure supercritical fluids turbulence. Finally, the methodology presented will be also utilized in the future to investigate the complex phenomenon of heat transfer improvement/deterioration in high-pressure transcritical fluids turbulence.

Acknowledgements

Funding sources

References

[1] L. Jofre and J. Urzay. A characteristic length scale for density gradients in supercritical monocomponent flows near pseudoboiling. *Annual Research Briefs, Center for Turbulence Research, Stanford University*, pages 277–282, 2020.

[2] L. Jofre and J. Urzay. Transcritical diffuse-interface hydrodynamics of propellants in high-pressure combustors of chemical propulsion systems. *Prog. Energy Combust. Sci.*, 82:100877, 2021.

[3] M. Bernades and L. Jofre. Thermophysical analysis of microconfined turbulent flow regimes at supercritical fluid conditions in heat transfer applications. *J. Heat Transfer*, 144:082501, 2022.

[4] J. Y. Yoo. The turbulent flows of supercritical fluids with heat transfer. *Annu. Rev. Fluid Mech.*, 45:495–525, 2013.

[5] M. Bernades, F. Capuano, and L. Jofre. Flow physics characterization of microconfined high-pressure transcritical turbulence. *Proceedings of the Summer Program 2022, Center for Turbulence Research, Stanford University*, pages 215–224, 2022.

[6] M. Bernades, F. Capuano, and L. Jofre. Microconfined high-pressure transcritical fluids turbulence. *Phys. Fluids*, 35:015163, 2023.

[7] F. Zhang, S. Marre, and A. Erriguible. Mixing intensification under turbulent conditions in a high pressure microreactor. *Chem. Eng. J.*, 382:122859, 2020.

[8] V. V. Lemanov, V. I. Terekhov, K. A. Sharov, and A. A. Shumeiko. An experimental study of submerged jets at low Reynolds numbers. *Tech. Phys. Letters*, 39:421, 2013.

[9] E. Buckingham. On physically similar systems; illustrations of the use of dimensional equations. *Phys. Rev.*, 4:345–376, 1914.

[10] A. M. Dunton, L. Jofre, G. Iaccarino, and A. Doostan. Pass-efficient methods for compression of high-dimensional turbulent flow data. *J. Comput. Phys.*, 423:109704, 2020.

26

[11] Z. R. del Rosario, M. Lee, and G. Iaccarino. Lurking variable detection via dimensional analysis. *SIAM-ASA J. Uncertain. Quan.*, 7(1):232–259, 2019.

[12] P. G. Constantine, Z. R. del Rosario, and G. Iaccarino. Data-driven dimensional analysis: algorithms for unique and relevant dimensionless groups. *arXiv preprint arXiv:1708.04303*, 2017.

[13] L. Jofre, Z. R. del Rosario, and G. Iaccarino. Data-driven dimensional analysis of heat transfer in irradiated particle-laden turbulent flow. *Int. J. Multiph. Fl.*, 125:103198, 2020.

[14] D. Y. Peng and D. B. Robinson. A new two-constant equation of state. *Ind. Eng. Chem. Fundam.*, 15:59–64, 1976.

[15] W. C. Reynolds and P. Colonna. *Thermodynamics: Fundamentals and Engineering Applications.* Cambridge University Press, Cambridge (UK), 1st edition, 2019.

[16] A. Burcat and B. Ruscic. Third millennium ideal gas and condensed phase thermochemical database for combustion with updates from active thermochemical tables. Technical report, Argonne National Laboratory, 2005.

[17] T. H. Chung, L. L. Lee, and K. E. Starling. Applications of kinetic gas theories and multiparameter correlation for prediction of dilute gas viscosity and thermal conductivity. *Ind. Eng. Chem. Fund.*, 23:8–13, 1984.

[18] T. H. Chung, M. Ajlan, L. L. Lee, and K. E. Starling. Generalized multiparameter correlation for nonpolar and polar fluid transport properties. *Ind. Eng. Chem. Fund.*, 27:671–679, 1988.

[19] B. E. Poling, J. M. Prausnitz, and J. P. O'Connell. *Properties of Gases and Liquids.* McGraw Hill, New York (USA), 5th edition, 2001.

[20] S. Gottlieb, C.-W. Shu, and E. Tadmor. Strong stability-preserving high-order time discretization methods. *SIAM Review*, 43:89–112, 2001.

[21] G. Coppola, F. Capuano, S. Pirozzoli, and L. de Luca. Numerically stable formulations of convective terms for turbulent compressible flows. *J. Comput. Phys.*, 382:86–104, 2019.

[22] G. Coppola, F. Capuano, and L. de Luca. Discrete energy-conservation properties in the numerical simulation of the navier-stokes equations. *Appl. Mech. Rev.*, 71(1), 2019.

[23] M. Bernades, F. Capuano, F. X. Trias, and L. Jofre. Energy-preserving stable computations of high-pressure supercritical fluids turbulence. In *9th European Congress on Computational Methods in Applied Sciences and Engineering (ECCOMAS)*, pages 1–12, 2022.

[24] M. Bernades, L. Jofre, and F. Capuano. Investigation of a novel numerical scheme for high-pressure supercritical fluids turbulence. *Proceedings of the Summer Program 2022, Center for Turbulence Research, Stanford University*, pages 225–234, 2022.

[25] T. M. Russi. *Uncertainty quantification with experimental data and complex system models*. PhD thesis, University of California Berkeley, 2010.

[26] P. G. Constantine. *Active Subspaces: Emerging Ideas for Dimension Reduction in Parameter Studies*. SIAM, Philadelphia (USA), 1st edition, 2015.

[27] M. Lee and R. D. Moser. Direct numerical simulation of turbulent channel flow up to $Re_\tau \approx 5200$. *J. Fluid. Mech.*, 774:395–415, 2015.

[28] M. Chevalier, J. Hœffner, T. R. Bewley, and D. S. Henningson. State estimation in wall-bounded flow systems. Part 2. turbulent flows. *J. Fluid Mech.*, 552:167–187, 2006.

[29] K. S. Pitzer, D. Z. Lippmann, R. F. Curl, C. M. Huggins, and D. E. Petersen. The volumetric and thermodynamic properties of fluids. II. Compressibility factor, vapor pressure and entropy of vaporization. *J. Am. Chem. Soc.*, 77:3433–3440, 1955.

[30] L. Jofre, A. Abdellatif, and G. Oyarzun. RHEA - an open-source Reproducible Hybrid-architecture flow solver Engineered for Academia. *J. Open Source Softw.*, 8(81):4637, 2023.

[31] P. T. Roy, L Jofre, J. C. Jouhaud, and B. Cuenot. Versatile sequential sampling algorithm using Kernel Density Estimation. *Eur. J. Oper. Res.*, 284:201–211, 2020.

[32] A. Firoozabadi. *Thermodynamics and Applications in Hydrocarbon Energy Production.* McGraw-Hill Education, New York (USA), 1st edition, 2016.

[33] S. Weisberg. *Applied Linear Regression.*